ELSEVIER

Available at
www.ElsevierMathematics.com
POWERED BY SCIENCE DIRECT®

Journal of Computational and Applied Mathematics 166 (2004) 123–131

JOURNAL OF COMPUTATIONAL AND APPLIED MATHEMATICS

www.elsevier.com/locate/cam

Boundary layer instability at the top of the Earth's outer core

Benoît Desjardins[a,*], Emmanuel Dormy[b], Emmanuel Grenier[c]

[a] *C.E.A./D.I.F., B.P. 12, Bruyères le Châtel, 91680 France*
[b] *I.P.G.P./C.N.R.S., 4 place Jussieu, Paris Cedex 05, 75252 France*
[c] *U.M.P.A., E.N.S. Lyon, 46 allée d'Italie, Lyon Cedex 07, 69364 France*

Received 6 September 2002; received in revised form 29 May 2003

Abstract

We investigate the instability of mixed Ekman–Hartmann boundary layers arising in rotating incompressible magnetohydrodynamics flows in a parameter regime relevant to the Earth liquid core. Relying on the small depth of the boundary layer, we perform a local study in a half-space at a given co-latitude $\theta \neq \pi/2$, and assume a mean dipolar axial magnetic field with internal sources (the geodynamo). Instabilities are driven, for high enough Reynolds number, by the quadratic term in the momentum equation.

Nonlinear stability can be proven using energy methods in the neighborhood of the poles (Nonlinearity 12 (2) (1999) 181). Next, following the work of Lilly (J. Atmos. Sci. 23 (1966) 481), we restrict our analysis to the linear growth phase. We describe the dependence of the critical Reynolds number in terms of θ and Elsasser number (measuring the relative strength of Lorentz and Coriolis forces). It turns out that no matter how large the Elsasser number is, there exists a critical band centered on the equator in which instabilities can occur. For geophysically relevant values of parameters, this band could extend as far as 45° away from the equator. This establishes the possibility of boundary layer instabilities near the Earth core-mantle boundary (CMB).

We finally present a first attempt of interaction with field maps at the CMB and core flows derived from the secular variation of the field, and discuss the sensitivity of the instability onset not only on the boundary layer Reynolds number, but also on the direction of the flow.

Keywords: Fluid dynamics; Magnetohydrodynamics; Boundary layers

* Corresponding author.
E-mail address: benoit.desjardins@cea.fr (B. Desjardins).

0377-0427/$ - see front matter
doi:10.1016/j.cam.2003.09.034

1. Introduction

The deep interior of our planet, namely its core, is essentially made of liquid iron. The magneto-hydrodynamic flow of this metal accounts for the generation of the Earth's magnetic field through a self-excited dynamo process. It is important in order to address the dynamics of this inductive process to better understand the dynamics of the boundary layer that forms as this metallic shell meets the solid mantle (about 3000 km below our feet). More specifically, this boundary layer is of an Ekman–Hartmann type (i.e., influenced both by rotation and magnetic field). We consider such boundary layers arising in rotating incompressible magnetohydrodynamic flows in a parameter regime relevant to the Earth liquid core.

One can try to model the core by a spherical shell Ω filled with a conducting fluid of density ρ, kinematic viscosity ν, conductivity σ, which rotates rapidly with angular velocity Ω_o. We will only consider here phenomena occurring close to the outer bounding sphere. Important parameters are the Ekman number E, the Rossby number ε, the magnetic Reynolds number R_m and the Elsasser number Λ defined introducing the magnetic diffusivity $\eta = (\sigma\mu_o)^{-1}$, a typical velocity U, length scale L and magnetic field $\mathscr{B}$ as

$$E = \frac{\nu}{2\Omega_o L^2}, \quad \varepsilon = \frac{U}{2\Omega_o L}, \tag{1}$$

$$R_m = \frac{UL}{\eta}, \quad \Lambda = \frac{\mathscr{B}^2}{2\rho\Omega_o\mu_o\eta}. \tag{2}$$

Physically, the Ekman number E can be interpreted as the ratio of the typical time scale for rotation τ_Ω (i.e., the day) to the viscous time scale τ_ν; the Rossby number ε corresponds to the ratio of τ_Ω to the typical advection time scale τ_U; the magnetic Reynolds number R_m represents the ratio of the magnetic diffusion time scale τ_η to τ_U; finally, the Elsasser number Λ is defined as the more complicated combination $\tau_\Omega\tau_\eta/\tau_A^2$, where τ_A denotes the typical time scale for Alfven waves.

We perform a local study in a half space at a given co-latitude $\theta \neq \pi/2$. The conducting liquid iron is assumed to be governed by the incompressible Navier–Stokes equations coupled with Maxwell's equations, in which displacement currents are neglected (magnetohydrodynamics approximation). Outside the Earth core, the mantle Ω^c is considered as an electrical insulator and the magnetic field is therefore harmonic.

At the core-mantle boundary $\partial\Omega$, we require the velocity of the fluid to vanish and the tangential component of the electric field and magnetic field to be continuous. Since we consider perturbations of a mean dipolar magnetic field $\mathbf{B}_o$, we split $\mathbf{B}$ into two parts $\mathbf{B} = \mathbf{B}_o + R_m\mathbf{b}$, where $\mathbf{b}$ denotes the scaled perturbation. Thus, the equations are written as follows:

$$\partial_t\mathbf{u} + \mathbf{u}\cdot\nabla\mathbf{u} + \frac{\nabla p}{\varepsilon} - \frac{E}{\varepsilon}\Delta\mathbf{u} + \frac{\mathbf{e}_\Omega\times\mathbf{u}}{\varepsilon} = \frac{\Lambda}{\varepsilon}\operatorname{curl}\mathbf{b}\times\mathbf{B} + \frac{\Lambda R_m}{\varepsilon}\operatorname{curl}\mathbf{b}\times\mathbf{b}, \tag{3}$$

$$\partial_t\mathbf{b} + \mathbf{u}\cdot\nabla\mathbf{b} = \mathbf{b}\cdot\nabla\mathbf{u} + \frac{\operatorname{curl}\mathbf{u}\times\mathbf{B}_o}{R_m} + \frac{\Delta\mathbf{b}}{R_m}, \tag{4}$$

$$\operatorname{div}\mathbf{u} = 0, \quad \operatorname{div}\mathbf{b} = 0, \tag{5}$$

and in Ω^c,

$$\operatorname{curl}\mathbf{b}=0,\quad \operatorname{curl}\mathbf{E}=-R_m\partial_t\mathbf{b}, \tag{6}$$

$$\operatorname{div}\mathbf{E}=0,\quad \operatorname{div}\mathbf{b}=0. \tag{7}$$

We consider in what follows the following orderings for $E,\Lambda,R_m,\varepsilon$:

$$\varepsilon\to 0,\quad \Lambda=\mathcal{O}(1),\quad \varepsilon R_m\to 0,\quad E\sim\varepsilon^2. \tag{8}$$

These limits are relevant for the Earth's core, for which we use the following estimates:

$$\mathscr{B}\sim 5\times 10^5\ \text{nT},\quad \rho\sim 10^4\ \text{kg m}^{-3},\quad \mu_o\sim 4\pi\times 10^{-7}\ \text{T m A}^{-1},\quad \eta\sim 1.1\ \text{m}^2\ \text{s}^{-1},$$
$$\nu\sim 10^{-6}\ \text{m}^2\ \text{s}^{-1},\quad \Omega\sim 7.3\times 10^{-5}\ \text{rad s}^{-1},\quad U\sim 10^{-4}\ \text{m s}^{-1}. \tag{9}$$

This yields nondimensional numbers of

$$\Lambda\sim 0.25,\quad \varepsilon\sim 4\times 10^{-7},\quad \sim 1.1\times 10^{-15},$$
$$R_m\sim 3.1\times 10^2,\quad Re_o\sim 16.8. \tag{10}$$

2. Nonlinear stability

First [2], we rigorously prove the nonlinear stability, provided the Reynolds number defined on boundary layer characteristics (see Eq. (23)) is smaller than a critical value. It is shown that the normal component of the magnetic field increases the critical Reynolds number for instability and that the nonlinear stability cannot be established everywhere at the Earth's core surface.

Let us first introduce the method on the pure Ekman case ($\Lambda=0$):

$$\varepsilon(\partial_t\mathbf{u}+\mathbf{u}\cdot\nabla\mathbf{u})+\nabla p-E\Delta\mathbf{u}+\mathbf{e}_\Omega\times\mathbf{u}=0, \tag{11}$$

$$\operatorname{div}\mathbf{u}=0,\quad \mathbf{u}_{|z=0}=0, \tag{12}$$

where

$$E\sim\varepsilon^2\to 0,\quad \beta=\frac{E^{1/2}}{\varepsilon}. \tag{13}$$

In the interior, away from the boundary

$$\partial_t\mathbf{u}_o^{\text{int}}+\mathbf{u}_o^{\text{int}}\cdot\nabla\mathbf{u}_o^{\text{int}}+\beta\mathbf{u}_o^{\text{int}}+\nabla p=0, \tag{14}$$

$$\operatorname{div}\mathbf{u}_o^{\text{int}}=0,\quad \mathbf{u}_o^{\text{int}}\cdot\mathbf{n}_{|z=0}=0. \tag{15}$$

Nonlinear stability will be proven in the following way:

$$\sup_{t\geqslant 0}\int|\mathbf{u}(t)-\mathbf{u}^{\text{int}}|^2\leqslant C\int|\mathbf{u}(0)-\mathbf{u}^{\text{int}}(0)|^2. \tag{16}$$

The main idea of the proof lies on a formal asymptotic expansion of the solution

$$\mathbf{u}\sim\mathbf{u}_N=\sum_{k=0}^{N}\varepsilon^k\left(\mathbf{u}_k^{\text{int}}(t,x,y,z)+\mathbf{u}_k^{\text{BL}}\left(t,x,y,\frac{z}{E^{1/2}}\right)\right). \tag{17}$$

An approximate solution satisfies:

$$\varepsilon(\partial_t \mathbf{u}_N + \mathbf{u}_N \cdot \nabla \mathbf{u}_N) + \nabla p_N - E\Delta \mathbf{u}_N + \mathbf{e} \times \mathbf{u}_N = \mathrm{O}(\varepsilon^{N+1}), \tag{18}$$

$$\operatorname{div} \mathbf{u}_N = 0, \quad \mathbf{u}_{N|z=0} = 0. \tag{19}$$

The next step is to estimate the energy of the difference $\mathbf{v} = \mathbf{u} - \mathbf{u}_N$:

$$\frac{\mathrm{d}}{\mathrm{d}t} \int \frac{|\mathbf{v}|^2}{2} + \frac{E}{\varepsilon} \int |\nabla \mathbf{v}|^2 \leqslant \left| \int \mathbf{v} \cdot (\mathbf{u} \cdot \nabla \mathbf{u} - \mathbf{u}_N \cdot \nabla \mathbf{u}_N) \right| + \cdots \tag{20}$$

$$\leqslant C \sup_{z \geqslant 0} \left| z \mathbf{u}^{\mathrm{BL}} \left(\frac{z}{E^{1/2}} \right) \right| \int |\nabla \mathbf{v}|^2 + \ldots \tag{21}$$

$$\leqslant C E^{1/2} \sup |\mathbf{u}^{\mathrm{int}}| \int |\nabla \mathbf{v}|^2 + \cdots \ . \tag{22}$$

Then, a stability criterium can be deduced

$$Re_{\mathrm{Ekman}} = \frac{\varepsilon \sup |\mathbf{u}^{\mathrm{int}}|}{E^{1/2}} = \frac{\varepsilon}{E} \sup |\mathbf{u}^{\mathrm{int}}| E^{1/2} = \frac{U L_{\mathrm{Ekman}}}{\nu} \leqslant Re_{\mathrm{c}}, \tag{23}$$

where $L_{\mathrm{Ekman}} = E^{1/2}$ denotes the size of the Ekman boundary layer.

In the general case, one gets

$$Re_{\mathrm{BL}} = \frac{|\mathbf{U}^{\mathrm{BL}}|_\infty L^{\mathrm{BL}}}{\nu} \leqslant Re_{\mathrm{c}}^{\mathrm{BL}}. \tag{24}$$

For the Ekman–Hartmann case ($\Lambda \neq 0$), the hydrodynamics is now coupled to the induction equation. The equation away from the boundary can be again written as

$$\partial_t \mathbf{u}_{\mathrm{o}}^{\mathrm{int}} + \mathbf{u}_{\mathrm{o}}^{\mathrm{int}} \cdot \nabla \mathbf{u}_{\mathrm{o}}^{\mathrm{int}} + \beta \mathbf{u}_{\mathrm{o}}^{\mathrm{int}} + \nabla p = 0, \tag{25}$$

$$\operatorname{div} \mathbf{u}_{\mathrm{o}}^{\mathrm{int}} = 0, \quad \mathbf{u}_{\mathrm{o}}^{\mathrm{int}} \cdot \mathbf{n}_{|z=0} = 0 \tag{26}$$

with

$$\beta = \sqrt{\frac{2E}{\varepsilon^2 \tan(\tau/2)}}, \tag{27}$$

$$\tan \frac{\tau}{2} = \frac{1}{\Lambda + \sqrt{1 + \Lambda^2}}. \tag{28}$$

As a result, the Ekman–Hartmann layer is stable if

$$\|U_\infty\| \frac{\varepsilon}{\sqrt{E}} \leqslant Re_{\mathrm{s}}(\Lambda, \theta), \tag{29}$$

since then

$$\sup_{t \geqslant 0} \int \left(|\mathbf{u}(t) - \mathbf{u}_{\mathrm{s}}|^2 + \frac{\Lambda R_{\mathrm{m}}}{\varepsilon} |b(t) - b_{\mathrm{s}}|^2 \right) \leqslant \int \left(|\mathbf{u}(0) - \mathbf{u}_{\mathrm{s}}|^2 + \frac{\Lambda R_{\mathrm{m}}}{\varepsilon} |b(0) - b_{\mathrm{s}}|^2 \right). \tag{30}$$

This expression is illustrated in Fig. 1 (see [2] for detailed analysis).

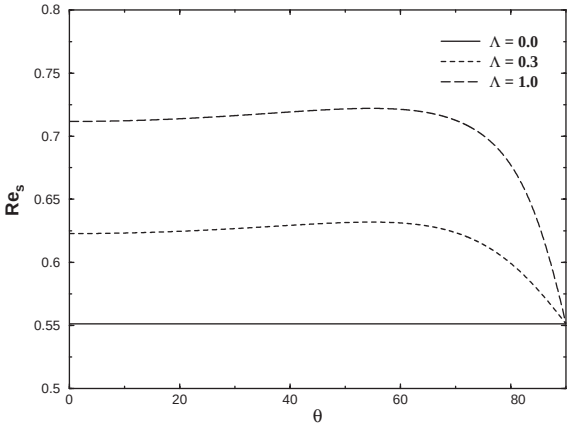

Fig. 1. Representation of the analytical nonlinear stability results (Re_s). If the Reynolds number Re attached to the boundary layer is lower than Re_s, nonlinear stability is demonstrated. We concentrate in the sequel on boundary layer Reynolds number above Re_s.

3. Linear instability

We now numerically investigate the linear instability of the layer. We study the dependence of the critical Reynolds number in terms of latitude and the Elsasser number (which measures the relative strength of Lorentz forces and Coriolis forces). We consider the linearized system (where λ denotes the boundary layer's scale)

$$\frac{\varepsilon}{\lambda}(\partial_t \mathbf{u} + \mathbf{U}\cdot\nabla\mathbf{u} + \mathbf{u}\cdot\nabla\mathbf{U}) - \frac{E}{\lambda^2}\Delta\mathbf{u} + \frac{\nabla p}{\lambda} = \frac{\Lambda}{\lambda}(\operatorname{curl}\mathbf{b})\times\mathbf{e}'$$
$$-\mathbf{e}\times\mathbf{u} + \frac{\Lambda R_m}{\lambda}((\operatorname{curl}\mathbf{B})\times\mathbf{b} + (\operatorname{curl}\mathbf{b})\times\mathbf{B}), \tag{31}$$

$$\frac{R_m}{\lambda}(\partial_t\mathbf{b} + \mathbf{U}\cdot\nabla\mathbf{b} + \mathbf{u}\cdot\nabla\mathbf{B} - \mathbf{b}\cdot\nabla\mathbf{U} - \mathbf{B}\cdot\nabla\mathbf{u}) = \frac{1}{\lambda}\operatorname{curl}(\mathbf{u}\times\mathbf{e}') + \frac{1}{\lambda^2}\Delta\mathbf{b}, \tag{32}$$

$$\operatorname{div}\mathbf{u} = 0, \quad \operatorname{div}\mathbf{b} = 0, \tag{33}$$

and seek travelling wave type solutions ($f(z)\exp(i\alpha(y' - ct))$). Angles are specified in Fig. 2. We want to minimize Re_i depending on the parameters α, γ, θ.

In the case $\theta = 0$ and in the absence of electromagnetic coupling, Lilly [5] showed that the Ekman flow is linearly unstable to two-dimensional disturbances when the Reynolds number $Re_o = \varepsilon\sqrt{2/E}$ exceeds the critical value 54.16. Our purpose is to extend Lilly's results to incompressible MHD flows at a given co-latitude $\theta \in [0, \pi/2)$ for a dipolar static magnetic field.

After validation of the critical values against Lilly's study and Leibovich and Lele [4], we obtain [3] the variation of the critical Reynolds number Re_i for instability with co-latitude (Fig. 3a). The angle for the travelling wave solution with $\mathbf{e}_\theta$ (namely δ) is represented in Fig. 3b. Note the bifurcation in two branches past a critical co-latitude (as observed in the nonmagnetic case by Leibovich and Lele).

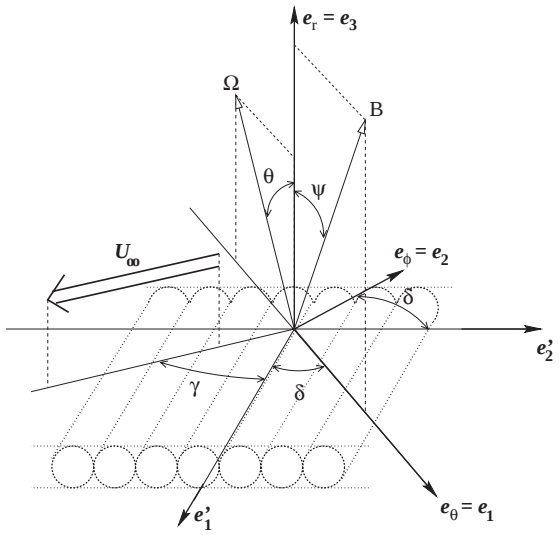

Fig. 2. Geometry of the local study. Rotation vector and magnetic field, respectively, make an angle θ and ψ with the normal to the boundary. Travelling wave solutions are sought for an external velocity $\mathbf{U}_\infty$. These quantities respectively make an angle δ and $\delta + \gamma$ with the plane $(\mathbf{\Omega}, \mathbf{B})$.

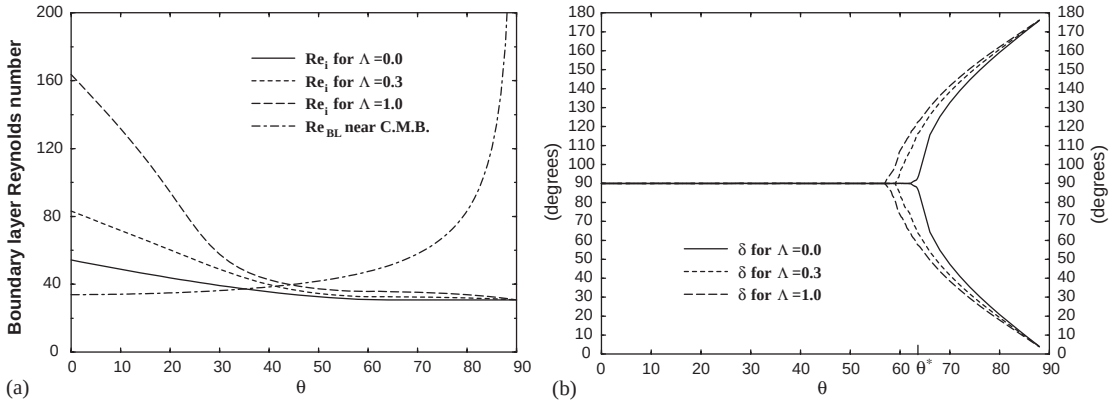

Fig. 3. (a) Boundary layer Reynolds number for instability for three different values of the Elsasser number versus co-latitude θ. An estimation of the boundary layer Reynolds number near the core-mantle boundary is also represented for comparison. (b) The direction at which the instability develops makes an angles δ with respect to e_θ; this is represented here versus the co-latitude θ. The instability develops in the e_ϕ direction near the pole. Past a critical co-latitude (decreasing with Λ) two branches of solutions exist. The instability is aligned with e_θ near the equator.

4. Linear instability from modeled large scale flow over the years

We finally present a first attempt of interaction with field maps at the Earth core-mantle boundary (CMB) and core flows derived from the secular variation of the field. Because the mantle is insulating, the principal field as measured in observatories can be expanded in spherical harmonics and

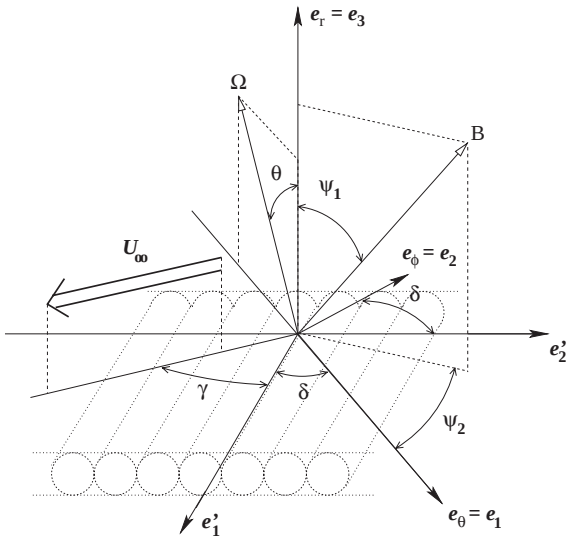

Fig. 4. Geometry for the local instability study based on actual magnetic field and core flow models. An additional angle ψ_2 is added since the field is not purely dipolar axial.

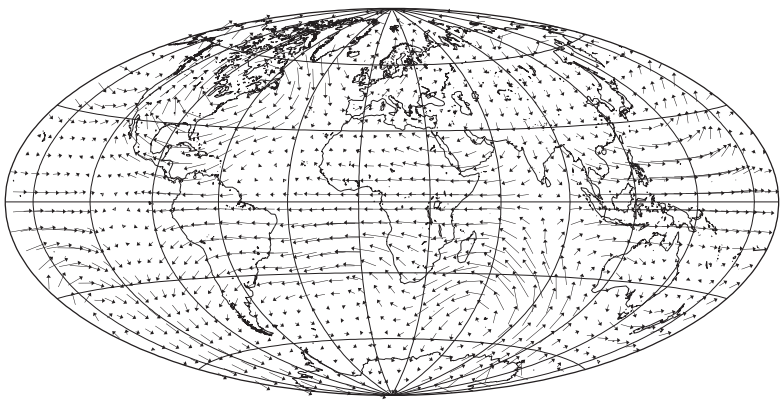

Fig. 5. The large scale velocity field near the core-mantle boundary can be reconstructed using magnetic field maps and their secular variation using the frozen flux approximation. It is here represented in 1980.

downward continued to the core surface, i.e., the boundary where we seek instabilities (see [1]). Consecutive models in time suggest a surface flow is required to account for the field variations (additional hypothesis are however needed to ensure uniqueness of this reconstructed flow: the flow is assumed to be of large scale and tangentially geostrophic). Such flow is represented in Fig. 5 for the year 1980 (e.g., [6]).

The model needs to include an additional angle ψ_2, now that the magnetic field does not necessarily lie in the meridional plane (the angle ψ_2 is defined in Fig. 4). The maximized growth rate together with the velocity field are computed.

Again we consider travelling wave type perturbations of the form $f(z)\exp(\mathrm{i}\alpha(y'-ct))$ for the velocity and magnetic field. Using the divergence free condition yields the existence of current functions $\tilde{\phi}$, $\tilde{\chi}$ such that $u_2 = -\partial_z\tilde{\phi}$, $u_3 = \partial_y\tilde{\phi}$, $b_2 = -\lambda\partial_z\tilde{\chi}$, $b_3 = \lambda\partial_y\tilde{\chi}$, where λ denotes the size of the Ekman–Hartmann boundary layer. Thus, $\tilde{\phi}$, $\tilde{\chi}$, u_1 and b_1 can be rewritten as follows:

$$\tilde{\phi}(t,y,z) = \phi(z)\mathrm{e}^{\mathrm{i}\alpha(y-ct)}, \quad \tilde{\chi}(t,y,z) = \chi(z)\mathrm{e}^{\mathrm{i}\alpha(y-ct)}, \tag{34}$$

$$u_1(t,y,z) = \mu(z)\mathrm{e}^{\mathrm{i}\alpha(y-ct)}, \quad b_1(t,y,z) = \beta(z)\mathrm{e}^{\mathrm{i}\alpha(y-ct)}. \tag{35}$$

The set of differential equations governing these perturbations can be written as

$$\begin{aligned} ci\alpha Re(\phi'' - \alpha^2\phi) = &-(\phi'''' - 2\alpha^2\phi'' + \alpha^4\phi) + 2\tan\frac{\tau}{2}(-\mu' + \mathrm{i}\alpha\tan\theta\sin\delta\mu) \\ &+\mathrm{i}\alpha V\, Re(\phi'' - \alpha^2\phi) - \mathrm{i}\alpha\, Re\, V''\phi \\ &-(1-\tan^2\frac{\tau}{2})(\chi''' - \alpha^2\chi' + \mathrm{i}\alpha\tan\psi_1\sin(\delta+\psi_2)(\chi'' - \alpha^2\chi)), \end{aligned} \tag{36}$$

$$\begin{aligned} ci\alpha Re\mu = &-(\mu'' - \alpha^2\mu) + 2\tan\frac{\tau}{2}(\phi' - \mathrm{i}\alpha\tan\theta\sin\delta\phi) + \mathrm{i}\alpha Re(V\mu + U'\phi) \\ &-\left(1-\tan^2\frac{\tau}{2}\right)(\beta' + \mathrm{i}\alpha\tan\psi_1\sin(\delta+\psi_2)\beta), \end{aligned} \tag{37}$$

$$\mathrm{i}\alpha\tan\psi_1\sin(\delta+\psi_2)\mu + \mu' + \beta'' - \alpha^2\beta = 0, \tag{38}$$

$$\mathrm{i}\alpha\tan\psi_1\sin(\delta+\psi_2)(\phi'' - \alpha^2\phi) + \phi''' - \alpha^2\phi' + \chi'''' - 2\alpha^2\chi'' + \alpha^4\chi = 0. \tag{39}$$

The z dependent profiles U and V are given by

$$U(z) = \cos\gamma_\mathrm{o} - \mathrm{e}^{-z}\cos\left(z\tan\frac{\tau}{2} + \gamma_\mathrm{o}\right), \quad V(z) = -\sin\gamma_\mathrm{o} + \mathrm{e}^{-z}\sin\left(z\tan\frac{\tau}{2} + \gamma_\mathrm{o}\right), \tag{40}$$

where

$$\tan\frac{\tau}{2} = \frac{\cos\theta}{\Lambda\cos^2\psi_1 + (\Lambda^2\cos^4\psi_1 + \cos^2\theta)^{1/2}}. \tag{41}$$

These profiles also depend on γ_o, minimization over γ_o is thus required to get the most unstable configuration.

As expected from the results of the previous section, we observe on preliminary computations that the most unstable zone is located in a neighborhood of the equator. The instability also appears to be confined to the Pacific ocean. The flow $\mathbf{U}_\infty$ we used as an input (5) has different directions depending on the hemisphere (Pacific/Atlantic). A study of the critical Reynolds number for instability (see Section 3) for a fixed latitude (here 10^o) but varying $\gamma_\mathrm{o}=\gamma+\delta$ (instead of looking for the minimizing value) reveals the lack of symmetry between eastward and westward flow. Indeed while the Reynolds number for instability corresponding to an imposed flow at $\gamma_\mathrm{o}=100^\mathrm{o}$ is less than 50, the corresponding value for $\gamma_\mathrm{o} = -100^\mathrm{o}$ exceeds 300 (Fig. 6). This explains why the unstable region appears under the Pacific Hemisphere, where the flow is eastward (see Fig. 5). The precise description of this instability together with its time dependence is postponed to a forthcoming study.

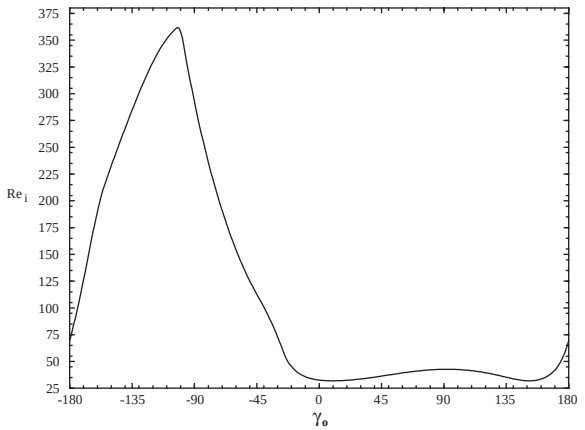

Fig. 6. We vary the angle $\gamma_o = \gamma + \delta$ for a fixed latitude of 10^o. The antisymmetry between eastward and westward flow is clear from the variation of the boundary layer Reynolds number for instability (Re_i).

5. Conclusion

Rather unexpectedly theory of boundary layer instabilities find interesting application in the Earth's internal dynamics. The existence of boundary layer instabilities at the top of the Earth liquid core provides a nice connection between this branch of applied mathematics and geophysics. The very small boundary layers (about a meter thick once scaled back to physical dimensions) are usually thought to be of little importance to the Earth's deep interior dynamics; such instabilities could severely alter this picture. Numerical models of geodynamo should take this effect into account. This disparity of scales (3×10^6 m for the largest scale and 1 m for the layer before the instability can develop) clearly highlights the difficulty of this problem.

References

[1] J. Bloxham, A. Jackson, Time-dependent mapping of the magnetic field at the core mantle boundary, J. Geophys. Res. 97 (1992) 19537–19564.

[2] B. Desjardins, E. Dormy, E. Grenier, Stability of mixed Ekman–Hartmann boundary layers, Nonlinearity 12 (2) (1999) 181–199.

[3] B. Desjardins, E. Dormy, E. Grenier, Instability of Ekman–Hartmann boundary layers, with application to the fluid flow near the core-mantle boundary, Phys. Earth and Planet. Inter. 123 (2001) 15–27;
B. Desjardins, E. Dormy, E. Grenier, Phys. Earth and Planet. Inter. 124 (2001) 283–294.

[4] S. Leibovich, S.K. Lele, The influence of the horizontal component of the Earth's angular velocity on the instability of the Ekman layer, J. Fluid Mech. 150 (1985) 41–87.

[5] D.K. Lilly, On the instability of Ekman boundary layer flow, on the instability of the Ekman boundary layer, J. Atmos. Sci. 23 (1966) 481–494.

[6] M.A. Faria Pais, Sur quelques mouvements animant le noyau terrestre, Ph.D. Thesis, Institut de Physique du Globe de Paris, 1999.